JACS
JOURNAL OF THE AMERICAN CHEMICAL SOCIETY

Article

pubs.acs.org/JACS

Solvent Driving Force Ensures Fast Formation of a Persistent and Well-Separated Radical Pair in Plant Cryptochrome

Gesa Lüdemann,[†] Ilia A. Solov'yov,*[,‡] Tomáš Kubař,[†] and Marcus Elstner*[,†]

[†]Department for Theoretical Chemical Biology, Institute for Physical Chemistry, Karlsruhe Institute of Technology, Kaiserstrasse 12, 76131 Karlsruhe, Germany

[‡]Department of Physics, Chemistry and Pharmacy, University of Southern Denmark, Campusvej 55, 5230 Odense M, Denmark

Supporting Information

ABSTRACT: The photoreceptor protein cryptochrome is thought to host, upon light absorption, a radical pair that is sensitive to very weak magnetic fields, endowing migratory birds with a magnetic compass sense. The molecular mechanism that leads to formation of a stabilized, magnetic field sensitive radical pair has despite various theoretical and experimental efforts not been unambiguously identified yet. We challenge this unambiguity through a unique quantum mechanical molecular dynamics approach where we perform electron transfer dynamics simulations taking into account the motion of the protein upon the electron transfer. This approach allows us to follow the time evolution of the electron transfer in an unbiased fashion and to reveal the molecular driving force that ensures fast electron transfer in cryptochrome guaranteeing formation of a persistent radical pair suitable for magnetoreception. We argue that this unraveled molecular mechanism is a general principle inherent to all proteins of the cryptochrome/photolyase family and that cryptochromes are, therefore, tailored to potentially function as efficient chemical magnetoreceptors.

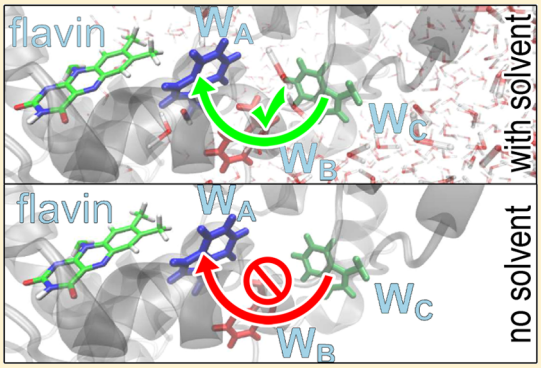

INTRODUCTION

Millions of animals, ranging from monarch butterflies,[1] salamanders,[2] sea turtles[3,4] to birds,[5,6] annually undertake remarkable migratory journeys, across oceans and through hemispheres, guided by the Earth's magnetic field. The cellular and molecular basis of this enigmatic sense, known as magnetoreception, remains an unsolved scientific mystery; some species use the magnetic sense as a compass to navigate entire oceans, others use it to detect geographic variations in the Earth's magnetic field to recognize their position.[7,8]

Migratory birds' magnetic sense seems to rely on the blue light photoreceptor protein cryptochrome, featured in Figure 1A,[10−18] found in the retina, the light-sensitive part of the eyes.[6,19] Cryptochrome is a signaling protein present in plants and animals.[20−22] Its role varies among organisms, from entrainment of circadian rhythms in vertebrates[23−25] to regulation of stem elongation in plants;[26,27] cryptochrome-containing cells within the retina are active when birds perform magnetic orientation.[6] Interestingly, cryptochrome controls a tidal rhythm in many species, based on a circalunar internal clock driven by night light, and many birds are nocturnal migrants[28−30] indeed.

Cryptochrome binds the chromophore flavin adenine dinucleotide (FAD) as a cofactor, see Figure 1B.[22,26,31−35] In plant cryptochromes from *Arabidopsis thaliana* (*A. thal.*),[31,36] FAD photoexcitation by blue light leads to conversion of fully oxidized FAD to a semireduced $FADH^{\bullet}$ radical form; the latter

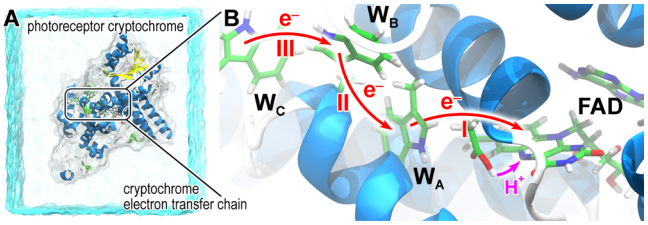

Figure 1. Cryptochrome structure and active site. (A) Structure of the protein cryptochrome-1 from *Arabidopsis thaliana*[9] in water environment. (B) Cryptochrome internally binds the flavin cofactor, which governs its signaling through light-induced electron (red arrows) and proton (magenta arrow) transfers involving a chain of three tryptophan residues, W_A, W_B, W_C. The three consecutive electron transfers $W_A \rightarrow FAD^*$, $W_B \rightarrow W_A^{\bullet+}$, and $W_C \rightarrow W_B^{\bullet+}$ are labeled I, II, and III, respectively.

represents the signaling state. The conversion happens in the course of light-induced electron transfer involving FAD and a chain of three tryptophan amino acid residues W_A, W_B, and W_C, see Figure 1B, which is found conserved throughout the entire cryptochrome/photolyase family.[22] For example, the tryptophan-triad in plant cryptochrome from *A. thal.* corresponds to the residues W400, W377, and W324, while in the *Drosophila*

Received: October 14, 2014
Published: December 23, 2014

DOI: 10.1021/ja510550g
J. Am. Chem. Soc. 2015, 137, 1147−1156

melanogaster (*D. mel.*) cryptochrome it is formed of W420, W397, and W342. Atomic structures of cryptochrome are known for *A. thal.*,[9] *D. mel.*[37,38] and *Mus musculus* (*M. musc.*).[39] In cryptochromes from insects, light excitation leads to formation of a flavin anion radical, $FAD^{\bullet -}$,[36] which may represent the signaling state in this case.[40]

Transient optical absorption and electron paramagnetic resonance spectroscopy[33−36,41,42] confirmed that vertebrate cryptochromes form long-lived intermediate states involving a flavin radical and a radical derived from a tryptophan residue. These radicals were shown to be likely responsible for a magnetic field effect observed in plant cryptochrome in vitro.[35] Unfortunately, little is known at present about structure of avian cryptochromes. Here, we focus, therefore, on photoactivation of plant cryptochrome, namely, from *A. thal.* with known structure.[9] Although the structure of bird and plant/insect/mammals cryptochromes are likely different, the proteins are homologous sequence-wise and, hence, their biophysical properties are expected to be closely related, in particular since the change of bird[5,43] and insect[1,44−46] behavior in magnetic field was reported; it has been established that fruit flies can respond to magnetic fields, but that cryptochrome knockout mutants cannot.

In the quest for explaining the avian magnetic sense, two mechanisms have attracted most attention. One mechanism, not further pursued here, being highly controversial, supposedly explains the recognition of magnetic landmarks, i.e., of places where the geomagnetic field varies in strength and inclination, and involves magnetic particles in the bird's body.[14,47−54] The other mechanism is more robust and explains the magnetic compass sense, e.g., recognition of the direction toward the Earth's magnetic pole, and is thought to be based on a magnetic field-dependent electron-transfer reaction in the bird's eye.[10,11,13,15,17,55−57] This so-called radical pair reaction is conjectured to modulate the visual perception of a bird with respect to the geomagnetic field, thereby, serving as a compass.[11,55]

The general mechanism of a radical pair reaction[10] is shown in Figure 2: a pair of radicals (molecules with a single unpaired electron) $[F^{\bullet}\ W^{\bullet}]$ is formed, e.g., by a photoactivated electron transfer reaction, in an entangled state which may be either singlet (S) or triplet (T). However, radical pair formation in cryptochrome is expected to be of singlet character.[12,35] S and T radical pairs coherently interconvert under the influence of local magnetic fields arising from internal (hyperfine) magnetic interactions and the Zeeman interaction with an external magnetic field. Thus, the fractional yields of the two products and the lifetime of the radical pair become magnetic field-dependent. If the radical pair is immobilized, the tensorial nature of the hyperfine interaction implies a directionality in the response to an external magnetic field which provides the basis of a so-called chemical compass sensor.[10,11,17] In cryptochrome the product state is thought to be formed independent of the spin state while the recombination reaction occurs from the singlet state only.[35]

Radical pairs, indeed, could act as a magnetic compass; however, the formation and dynamics of radical pairs in cryptochromes from different organisms is not yet clearly resolved. Transient absorption and EPR spectroscopy can identify transient states in cryptochrome photoactivation process, and a computational route that describes cryptochrome photochemistry in atomistic details could add most valuably to this. However, results of the transient absorption

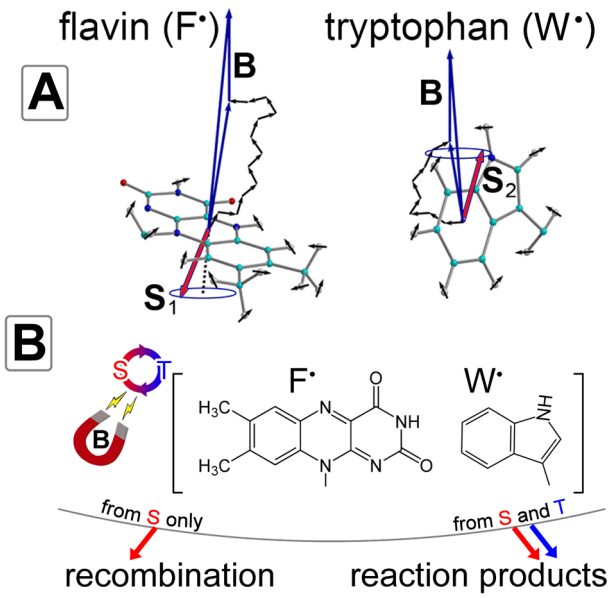

Figure 2. The radical pair mechanism. (A) Magnetic field effect on a radical pair involving flavin ($F^{\bullet}$) and tryptophan ($W^{\bullet}$) in cryptochrome. Unpaired electron spins (S_1 and S_2) precess about a local magnetic field due to external magnetic field **B** and nuclear spins on flavin and tryptophan. The spin precession continuously alters the relative orientation of S_1 and S_2 causing singlet $^{S}[F^{\bullet}\ W^{\bullet}]$ to triplet $^{T}[F^{\bullet}\ W^{\bullet}]$ interconversion, which underlies the magnetic field effect. (B) Radical pair reaction scheme. The state $^{S}[F^{\bullet}\ W^{\bullet}]$ is formed initially through electron transfer, as shown in Figure 1B. Arrows indicate spin-dependent radical pair reactions that could occur either from the singlet (red) or the triplet (blue) states of the radical pair. Recombination reaction corresponds to the electron back-transfer process in the $^{S}[F^{\bullet}\ W^{\bullet}]$ radical pair, while reaction product denote the reaction yield of the radical pair forward reaction.

measurement become increasingly complex to evaluate if several molecules absorb light simultaneously at the same wavelengths.

Furthermore, to establish the magnetoreceptor role of cryptochrome it is first necessary to reveal how the protein becomes biologically active. For this purpose, we have recently combined first-principles quantum chemistry and classical all-atom molecular dynamics (MD) simulations to investigate the photoreaction of plant cryptochrome.[55,56] The electron transfer studies focused on the static configurations of cryptochrome, taken from MD simulations of different cryptochrome radical pair states. The active site of the protein was studied quantum mechanically in its different possible electronic states. This study established the energies of possible electronic configurations of cryptochrome active site and suggested the possible transformations in cryptochrome upon its light photoexcitation. Thus, we have demonstrated that a radical pair involving flavin and a tryptophan residue $W_A(H)^{\bullet +}$, see Figure 1, is rapidly formed upon flavin photoexcitation, and could subsequently be stabilized through a proton transfer between positively charged W_A and negatively charged flavin involving as aspartic acid as an intermediate, see Figure 1. Further analysis of the electronic structure of the cryptochrome active site[55] demonstrated the possibility of a $W_B \rightarrow W_A^{\bullet +}$ electron transfer (transfer II in Figure 1) succeeding the $W_A \rightarrow FAD^*$ electron transfer (transfer I in Figure 1). The rate of transfer II was shown to be crucial as this transfer has to outrun flavin protonation; once flavin protonation takes place the closely spaced [$FADH^{\bullet}$ +

DOI: 10.1021/ja510550g
J. Am. Chem. Soc. 2015, 137, 1147−1156

$W_A^{\bullet}$] radical pair becomes stabilized and impedes transfer II energetically. The theoretical investigations[55,56] clearly confirmed that the sequential electron transfer in cryptochrome is feasible, supporting experimental observations,[32,35,42] but a more quantitative account of the protein environment on the electron dynamics at the active site was called for to complete the study.

Here, we undertake the final challenge to complete the description of the photoactivation of *A. thal.* cryptochrome and focus on the dynamical description of the electron transfer processes. We employ a multiscale computational approach, where the propagation of the electron on the tryptophan triad, according to the electronic Schrödinger equation, is coupled to the nuclear dynamics of the entire system.[58−60] This method has been applied successfully to understand the electron transfer dynamics in a cyclobutane pyrimidine dimer (CPD) photolyase recently.[61,62] We describe the electron transfer along the tryptophan triad in *A. thal.* cryptochrome quantum mechanically, taking into account the complete biological environment of the active site, which includes the protein matrix and the solvent around it, as shown in Figure 1A. These environment components have never been accounted in earlier computations, and are here demonstrated to be crucial for the efficient long-range and robust electron transport between the FAD cofactor and the protein surface. The performed computations capture the essentials of the reaction kinetics and thermodynamics and reveal the molecular mechanism of electron transfer in *A. thal.* cryptochrome, allowing direct simulations of electron transfer events on their natural time scale, as confirmed through an excellent agreement with experiment.[22,42] Free energy calculations are used to study the protonation reaction of flavin in greater detail, with account for its complete biological environment.

METHODS

Calculations were performed employing a combination of theoretical methods. MD simulations were performed with the GROMACS package[63] with the improved Amber99 force field.[64,65] The protonation reaction is modeled quantum mechanically by employing an approximate density functional theory (DFT) method in a combined quantum mechanics/molecular mechanics (QM/MM) potential of mean force (PMF) approach. QM/MM electron transfer simulations and QM/MM umbrella sampling simulations were performed with an in-house version of GROMACS 4.6 for the MM part and DFTB3[66] for the QM part. All images were rendered with VMD.[67]

Molecular Dynamics Simulation. The protein structure of *A. thal.* cryptochrome-1 used in this study is based on the X-ray crystal structure by Bräutigam et al. (PDB ID 1U3C).[9] The FAD cofactor was built from riboflavin and adenosine diphosphate (ADP) models using a force field parametrization developed earlier.[64,68] Atomic charges for both neutral FAD and negatively charged $FAD^{\bullet-}$ were determined from RESP calculations[69] and are provided in the Supporting Information (SI). Force field parameters for the tryptophan cation radical were obtained as described before.[61] The in situ pK_a value of the D396 side chain, determined with a MCCE[70] calculation was about 10; therefore, D396 was modeled as protonated. The protein model was solvated in a rectangular periodic box of $93 \times 101 \times 90$ Å^3 size filled with TIP3P water molecules;[71] neutralized with Na^+ ions, excess Na^+ and Cl^- were added to obtain a 50 mM solution of NaCl. All simulations were performed with the GROMACS package.[63] The improved Amber99 force field was used[64,65] for the protein parts. The structure of cryptochrome in its resting state obtained after a 100 ns MD simulation performed in an earlier investigation[56] was used as a starting configuration for the present simulation. These 100 ns were thus considered as an extended equilibration of the system, and were performed using the NAMD package[72] with the CHARMM27[73,74] force field. Finally, a 170 ns MD simulation was carried out. The integration time step was 2 fs. The temperature was kept at 300 K by applying the Nose−Hoover thermostat,[75] while the pressure was controlled by the Parinello−Rahman Barostat[76] at a value of 1 atm. The LINCS algorithm[77] was employed to keep bonds involving hydrogen atoms at a fixed length. The time evolution of the cryptochrome backbone root-mean-square deviation (RMSD) is shown in Figure S2, confirming the stability of the simulation.

An in-house version of GROMACS 4.6 with modifications were used to carry out the coupled QM/MM calculations during the dynamic electron transfer simulations and QM/MM umbrella sampling simulations. A time step of 1 fs was used in all QM/MM simulations.

Direct Electron Transfer. The populations of the radical pair states were obtained from nonadiabatic QM/MM MD simulations.[58] Here, the wave function of the transferring electron and the coordinates of all of the atoms in the system were propagated simultaneously by means of the time-dependent Schrödinger equation and of the classical Newton equations, respectively. The simulation scheme is based on the density functional theory (DFT) and was designed for high computational efficiency, so that quantum dynamics in proteins could routinely be probed on multinanosecond time scales. The electronic structure of the QM system is obtained with a fragment-orbital approach,[78] achieving effectively a linear scaling of the computational cost. The application of the approximative DFT method DFTB[79] also leads to computational time reduced by two to 3 orders of magnitude compared to conventional DFT, but still maintaining the necessary level of accuracy.

Importantly, the fragment-orbital QM/MM Hamiltonian of the system accounts for the entire protein and the solvent environment, and it is reevaluated in every step of the MD simulation, so that any response of the molecular environment to a change of the electron density is taken into account immediately. The response of molecular environment is made possible by an update of atomic charges in the classical MD simulation, which is performed in every MD step according to the spatial distribution of the transferring electron. Note that no assumptions are made a priori, neither about the time scales of electron transfer nor about the localization/delocalization of the electron in the system.

The direct electron transfer simulation framework is described briefly in the SI, and the reader may also refer to recent review publications for more details.[59,60] Previously, this scheme was applied to study the electron transfer in *Escherichia coli* photolyase successfully.[61,62] In the present investigation, the QM region includes the amino acid side chains in the *A. thal.* cryptochrome that are involved in the electron transfer directly, i.e., the side chains of tryptophans W400, W377 and W324, see Figure S1.

Density Functional Based Tight Binding Method. Density functional based tight binding method (DFTB) is a series of models derived from DFT, being about 2−3 orders of magnitude faster than the conventional DFT with medium-sized basis sets. DFTB2 is derived from a second-order Taylor expansion of the DFT total energy around a reference density. Recently,[66] DFTB has been extended to the third order, giving rise to the DFTB3 method, allowing a much more accurate description of proton affinities and hydrogen bonding energies.[80] Since the FAD molecule, relevant for the present investigation, was not included in the original test set,[80] the DFTB3 was tested for relative proton affinities of FAD and aspartate, and it was found that DFTB is an appropriate method for computing relative proton affinities with sufficiently high accuracy of about 2 kcal/mol, as compared to ab initio reference calculations: see Table S2 and the discussion in the SI for more details.

Umbrella Sampling. The free energy of FAD protonation via D396 was obtained with umbrella sampling simulations followed by a weighted histogram analysis (WHAM).[81] The starting geometries for the simulations in the individual umbrella sampling windows were taken from a QM/MM MD simulation performed with an additional harmonic potential that was being shifted gradually with a rate of 0.024 Å/ps. This slow pulling simulation gave rise to structures spanning the

DOI: 10.1021/ja510550g
J. Am. Chem. Soc. 2015, 137, 1147−1156

entire proton transfer path, avoiding unphysical distortions of the holo-protein structure. The reaction coordinate was defined as the distance between the hydrogen of D396 and N5 of the flavin group (see magenta arrow in Figure 1B). The starting point of the free energy calculation corresponds to a conformation with the COOH group of D396 turned entirely toward the flavin cofactor. The reaction coordinate was sampled from 2.6 Å down to 0.9 Å to span the transfer of the proton toward the N5 atom. Here, eight umbrella sampling windows with a spacing of 0.2 Å between 2.6 and 1.7 Å, and, additionally, seven umbrella sampling windows with 0.1 Å spacing from 1.6 to 0.9 Å were used. The force constant of the biasing potential was set to 100,000 kcal/mol/nm^2, and a QM/MM MD simulation of 150 ps was performed for each window.

RESULTS

Cryptochrome flavin photoexcitation triggers electron transfer along the tryptophan triad, see Figure 1B, leading to the formation of the radical pair [FAD$^{\bullet-}$+W(H)$^{\bullet+}$], possibly relevant for magnetoreception.[55] Transient absorption data and mutation studies identify the third tryptophan, which is located closest to the exterior of the protein as ultimate electron donor. We perform unbiased dynamic simulations of the electron transfer along the tryptophan triad in order to (i) identify the tryptophan which together with the FAD forms a persistent radical pair, and (ii) to reveal the underlying molecular mechanism of the photoactivation reaction in plant cryptochrome. The three tryptophans of the triad in *A. thal.* cryptochrome studied here are W400, W377 and W324,[32] and for the sake of simplicity in the following are denoted as W_A, W_B, and W_C, respectively, as also noted in Figure 1B. The corresponding radical pairs [FAD$^{\bullet-}$+W400(H)$^{\bullet+}$], [FAD$^{\bullet-}$+W377(H)$^{\bullet+}$] and [FAD$^{\bullet-}$+W324(H)$^{\bullet+}$] are thus labeled RP-A, RP-B and RP-C, respectively.

Electron Transfer Dynamics along the Tryptophan Triad. Figure 3 summarizes the results of electron transfer dynamics in cryptochrome and shows the population of the radical pair states RP-A, RP-B and RP-C over an interval of 1 ns. The population of a radical pair is a key quantity to define which tryptophan is forming a radical at a given time instance. Per definition, radical pair population varies between 0 and 1,

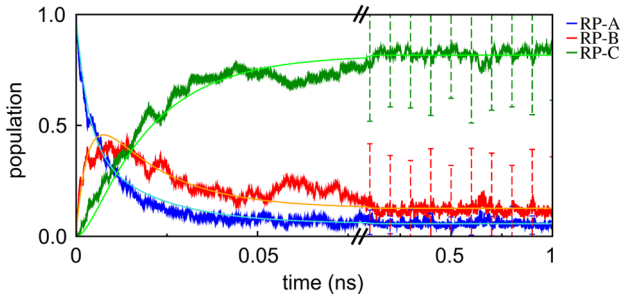

Figure 3. Formation and decay of three possible radical pair states in *A. thal.* cryptochrome. The initially occupied RP-A state (blue) decays rapidly giving rise to the RP-B state (red) followed by the formation of the RP-C state (green). The radical pair population is obtained as an ensemble average of 32 simulations of 1 ns length, which were calculated from snapshots taken from a MD simulation of the cryptochrome resting state at 500 ps intervals to represent the ensemble of cryptochrome structural variety. Error bars denote the standard deviation and indicate the variance of the time evolution of the population observed for the underlying individual simulations. The average populations (light blue, orange, light green lines) represent the fitting curves from a two-step kinetic model, eq 4, which has been fitted to the simulation data.

where 0 is characteristic for a neutral tryptophan, while 1 denotes the cation radical state. Initially, cryptochrome is assumed to be in the RP-A state, as the RP-A state is formed in less than a picosecond after flavin photoexcitation.[42] In the course of the simulation, the FAD cofactor remains negatively charged while the electron is free to move between W_A, W_B and W_C. As follows from Figure 3, the radical pair RP-A (blue) decays quickly, within 20 ps, giving rise to the formation of the RP-B state (red) and finally the RP-C state (green). The radical pair RP-B is only built up to about 40% when it starts decaying, giving rise to the population of the RP-C state. After 150 ps, the RP-C population remains stable at about 80% for the rest of the simulation. The observed behavior could be understood as a two-step electron transfer process with the transfer $W_B \rightarrow W_A(H)^{\bullet+}$ followed by a second transfer $W_C \rightarrow W_B(H)^{\bullet+}$ yielding RP-C as the ultimate radical pair. Video S1 in the SI illustrates how this process happens dynamically.

Note that after 1 ns, about 10% of RP-B still remains, indicating that there is a small but significant probability of RP-B stabilization. This observation is also supported by an analysis of the individual simulations, which showed that for 2 out of 32 simulations the electron has transferred from W_B to $W_A^{\bullet+}$ but not transferred on from W_C to $W_B^{\bullet+}$; see Video S2 in the SI for an illustration of RP-B stabilization. Characteristic examples of several individual simulations are illustrated in the Figure S3.

The results from the electron transfer dynamics simulation are in an excellent agreement with mutational studies of *A. thal.* cryptochrome-1,[32] which show a prominent role of the tryptophan triad for electron transfer and identify W_C as a likely candidate for the terminal electron donor. A residual activity of the W324 mutant observed in the experiment might be explained by the small but existing RP-B population seen in the present simulations.

The spatial separation of the radical pair is a crucial parameter for the weak magnetic field sensitivity,[10] as the dipole−dipole and exchange interactions between the radical partners become less relevant with increasing distance. The radical separation for RP-B is 12.2 Å while for RP-C it is 19.4 Å on average (the distances are considered between the centers of mass of the tryptophan side chain and the flavin isoalloxazine ring). The distance d(FAD···W_B) depends on the redox state of the protein and for the RP-B state turns out to be about 1.3 Å lower as compared to resting state of cryptochrome, while the distance d(FAD···W_C) for the RP-C state of cryptochrome increases by about 0.7 Å, see Table S1. The changes in the radical pair distances could most likely be attributed to a small rearrangement of the tryptophanes due to the solvent polarization by the moving electron. Importantly, both RP-B and RP-C exhibit a radical pair separation above the critical distance,[22,55] with RP-C being much more preferable for magnetoreception due to the larger distance.

To connect the results from the performed simulations with the available experimental data, we have conducted a numerical fit (see light color lines in Figure 3) of the average radical pair population according to a kinetic model that allows both forward and backward transfer reactions

$$W_A \underset{k_b^{II}}{\overset{k_f^{II}}{\leftrightarrows}} W_B \underset{k_b^{III}}{\overset{k_f^{III}}{\leftrightarrows}} W_C \qquad (1)$$

where k^{II} and k^{III} denote the rate constants for electron transfer steps II and III, see Figure 1B, and the subscripts f and b indicate the forward and backward transfers, respectively. The

DOI: 10.1021/ja510550g
J. Am. Chem. Soc. 2015, 137, 1147−1156

two-step kinetic process above including back transfer could be described with coupled rate equations:

$$\frac{d[A]}{dt} = -k_f^{II}[A] + k_b^{II}[B] \quad (2)$$

$$\frac{d[B]}{dt} = -k_f^{III}[B] + k_f^{II}[A] + k_b^{III}[C] \quad (3)$$

$$\frac{d[C]}{dt} = -k_b^{III}[C] + k_f^{III}[B] \quad (4)$$

Here, the square brackets [...] denote the normalized concentration of the corresponding radical pair, or in other words, the radical pair population. Since initially only RP-A was populated, the initial conditions for eqs 2−4 are

$$[A]|_{t=0} = 1;\ [B]|_{t=0} = 0;\ [C]|_{t=0} = 0. \quad (5)$$

Eqs 2−4 are solved numerically by varying the four rate constants k_f^{II}, k_b^{II}, k_f^{III}, k_b^{III} until the deviation of the average radical pair population from the simulation data points in Figure 3 is minimized. The final numerical fit of the radical pair population is shown in Figure 3 with light color lines, while the obtained rate constants are summarized in Table 1.

Table 1. Rate Constants of the Electron Transfer Steps in *A. thal.* Cryptochrome[a]

e⁻ transfer step	donor−acceptor	k_f [ns^{-1}]	k_b [ns^{-1}]
II	$W_B \rightleftarrows W_A$	190 ± 18	85 ± 18
III	$W_C \rightleftarrows W_B$	70 ± 18	10 ± 18

[a]The error bars denote the deviation of the numerical fit from the simulation data.

The rates of the electron transfers $W_B \rightarrow W_A^{\bullet+}$ and $W_C \rightarrow W_B^{\bullet+}$ are found to be 190 and 70 ns^{-1}, respectively. Since the rate $k_{W_B \rightarrow W_A^{\bullet+}}$ is more than twice as high as the rate $k_{W_B \rightarrow W_C^{\bullet+}}$, a two-step electron migration with a fast transfer $W_B \rightarrow W_A^{\bullet+}$ followed by a somewhat slower, but still fast transfer $W_C \rightarrow W_B^{\bullet+}$ is expected.

Note that the mean-field approach, used in our model to propagate the electron, suffers from electron overdelocalization, an effect which gradually increases over the course of a simulation. As a result the population of the less probable states RP-A and RP-B will be overestimated, while the population of the more probable state RP-C will be underestimated at the end of the 1 ns simulations. The overdelocalization could, thus, lead to an overestimate of the electron transfer rates by about an order of magnitude.

However, the derived electron transfer rates seem to be in an excellent agreement with the experimental kinetics obtained by Immeln et al.,[42] suggesting electron transfer from a tryptophan residue on the protein surface to the flavin to be completed by a 100 ps delay. The experimental kinetics[42] yielded three time constants. The time constant of 0.4 ps was assigned to the initial tryptophan-to-flavin electron transfer (transfer I in Figure 1B). The other two time constants 4−15 ps (rate constant 67−250 ns^{-1}) and 30−50 ps (rate constant 20−33 ns^{-1}) were both related to the rate of appearance of the tryptophan cation radical species. In the light of the present findings, the two experimental rate constants could be related to the faster electron transfer $W_B \rightarrow W_A^{\bullet+}$ followed by the comparably slower electron transfer $W_C \rightarrow W_B^{\bullet+}$ along the tryptophan triad.

Maeda et al.[35] obtained an estimate for the backtransfer rate k_b^{III} for transfer III (0.01 ns^{-1}) from fitting the experimental data to a quantum spin dynamics model, assuming that k_b^{III} is close to the singlet triplet dephasing rate. This estimate suggests, that the backtransfer rate k_b^{III} derived in the present study is overestimated, as it turns out to be 3 orders of magnitude higher. As argued above, the present calculation, indeed could lead to a somewhat larger value of the backtransfer rate, due to the electron overdelocalization arising in the mean-field approach. The estimated backtransfer rates should, therefore, be treated as a lower threshold values of the actual kinetic rates; however, the obtained values are still noticeably smaller than the forward rates, which suggests that electron backtransfer would be strongly suppressed in cryptochrome.

Driving Force for Electron Transfer along the Tryptophan Triad. The cryptochrome resting state does not have an appropriate potential energy surface (brought about, e.g., by a specific arrangement of charged amino acids around the tryptophan triad) that would energetically favor the sequential electron transfer. This has already been demonstrated on a purely quantum mechanical model of the active site, where rearrangements induced by charge separation were shown to be of crucial importance.[55,56] One then concludes that there is no permanent, resting state electrostatic potential resulting from protein and solvent electrostatic interactions. The electron transfer driving force rather occurs due to dynamic polarization of the environment by the electron.

To quantify the stabilization of each radical pair by the environment, we computed the relative energy of each radical pair with respect to the energy of the FAD-tryptophan pair in the charge neutral state. Figure 4 depicts the relative energies

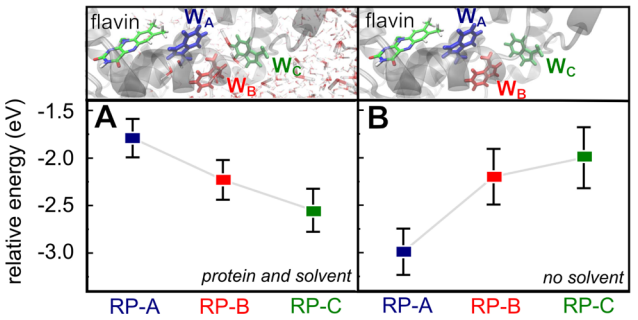

Figure 4. Contribution of the environment to the stabilization of each radical pair with respect to the charge neutral state. (A) The simulations including both protein and solvent environment show the average relative energy of the radical pairs to steadily decrease from RP-A to RP-C. (B) The average relative energy due to protein environment only, neglecting the effect of the solvent, increases from RP-A to RP-C. Since the relative energy is strongly coupled to protein environment and solvent, large fluctuations occur. Error bars denote the standard deviation.

averaged over 1 ns, including both protein and solvent environment (Figure 4A), and considering the protein environment only (Figure 4B). Figure 4A shows that all three radical pairs are stabilized by the polarized environment by more than 1.5 eV upon charge separation. However, the comparison of RP-A, RP-B and RP-C shows that the stabilization of each of the three radical pairs is different, with RP-C experiencing the strongest stabilization. The relative energy of RP-B is 0.44 eV lower compared to RP-A, and RP-C is even more stabilized by nearly 0.8 eV with respect to RP-A.

DOI: 10.1021/ja510550g
J. Am. Chem. Soc. 2015, 137, 1147−1156

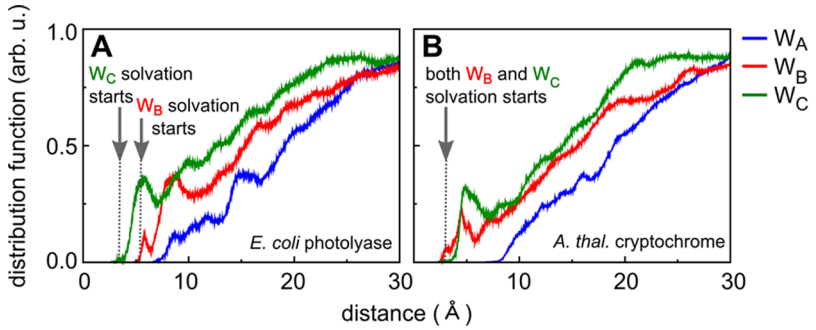

Figure 5. Radial distribution of water around the three tryptophans. The radial distribution function is a measure for the solvent accessibility of each tryptophan W_A (blue), W_B (red) and W_C (green) in the resting state for *E. coli* photolyase (A) and *A. thal.* cryptochrome (B). W_B is found to be better solvated in the case of *A. thal.* cryptochrome than in the case of *E. coli* photolyase. The Gromacs tool g_rdf was used to calculate the radial distribution functions.

These energy differences represent a driving force for electron transfer from W_C over W_B to $W_A^{\bullet+}$.

A similar effect has been reported for *E. coli* photolyase,[61] and it was found to result from stronger solvation of the outer tryptophan, which induced a stronger stabilization of the tryptophan cation radical due to a more favorable solvent repolarisation.

To assess the effect of solvent on electron transfer in cryptochrome in more detail, we excluded the QM/MM interaction of the water molecules and considered only the interaction with atoms from the protein environment, see Figure 4B. A completely different picture emerges: RP-A is stabilized most strongly, while RP-B and RP-C experience lesser stabilization, suggesting that the electron transfer steps II and III in Figure 1B would be hindered energetically. A similar observation was reported for cryptochrome using a quantum chemical approach for an active site model, i.e., neglecting the solvent and large parts of the environment.[56] There, an endothermic electron transfer process $W_B \rightarrow W_A^{\bullet+}$ was found, with a reaction energy of about +0.26 eV.

The performed analysis reveals clearly that the solvent plays an important role in *A. thal.* cryptochrome and is responsible for the strong driving force and exothermicity of the electron transfer process, inducing a predominant stabilization of the RP-C state.

Solvent Exposure of Individual Tryptophans. Since *E. coli* photolyase and *A. thal.* cryptochrome are activated similarly,[82] it is natural to compare the activation mechanisms of the two proteins. Comparing the degree of solvent exposure of the three tryptophans for cryptochrome and photolyase, a small but crucial difference is revealed. Photolyase shows a larger difference in solvation of W_B and W_C than observed in cryptochrome, with W_B being more buried inside the protein matrix. To quantify the solvent exposure of the individual tryptophans, it is useful to compute the radial distribution of water molecules around the three tryptophans. The radial distribution function defines the probability of observing a water molecule within a sphere of radius r from the respective tryptophan W_A, W_B or W_C. It is obtained by counting the number of water molecules found within this sphere for each time step along a MD trajectory, and normalizing it by the number of water molecules found in a sphere with a sufficiently large cutoff radius (here, 30 Å is used).

Figure 5 shows the radial distribution of water molecules around the three tryptophans of photolyase from the previous study[61] and the data calculated presently for cryptochrome. In the case of photolyase, the water distribution sets on at 5.5 Å for W_B and at 4 Å for W_C. In contrast, the distribution of water for cryptochrome tryptophans sets on at 4 Å for both residues. The higher maximum value for W_C in the case of cryptochrome indicates that a larger number of water molecules can be found at a distance up to 5 Å from W_C than in the vicinity of W_B. This still renders W_C the most solvated tryptophan of the triad in cryptochrome also, and explains qualitatively why RP-C is stabilized the best. However, the merely qualitative difference between RP-B and RP-C also hints to the nonzero probability of RP-B stabilization found in the dynamical electron transfer simulation for cryptochrome, which was never observed in *E. coli* photolyase.[61]

Structural Mechanism for RP-B Stabilization. For those simulations where RP-B became stabilized, and no $W_C \rightarrow W_B(H)^{\bullet+}$ electron transfer was possible (see Video S2), we have observed an increase of the center of mass distance between $W_B(H)^{\bullet+}$ and W_C by about 0.5 Å, and the electronic coupling between $W_B(H)^{\bullet+}$ and W_C showed a step-like decrease to nearly zero as can be seen in Figure 6A. The electronic coupling determines the probability of electron transfer between the tryptophans; a decrease of the electronic coupling means a drop of the probability of electron transfer between $W_B(H)^{\bullet+}$ and W_C. The difference between the conformations of the tryptophan pair is very subtle, see Figure 6B, still it may affect the electron transfer substantially: the low

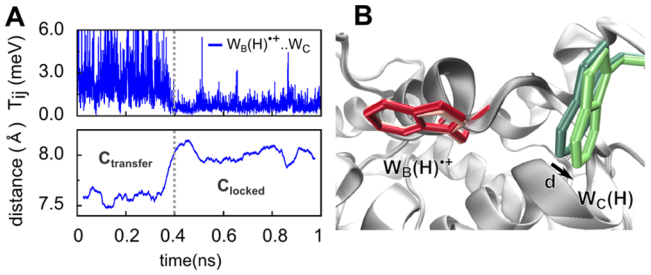

Figure 6. RP-B could be stabilized by a subtle rearrangement of W_C. (A) After about 400 ps, the distance between the center of mass of $W_B(H)^{\bullet+}$ and W_C increases (bottom), and the electronic coupling between $W_B(H)^{\bullet+}$ and W_C drops to almost zero (top). The drop of the electronic couplings makes vanish the probability for electron transfer $W_B \leftarrow W_C(H)^{\bullet+}$. (B) The increase of the distance between $W_B(H)^{\bullet+}$ and W_C gives rise to two conformations $C_{transfer}$ (light colors) and C_{locked} (dark colors). The two conformations $C_{transfer}$ and C_{locked} are obtained as average of the trajectory before and after 400 ps, respectively.

DOI: 10.1021/ja510550g
J. Am. Chem. Soc. 2015, 137, 1147−1156

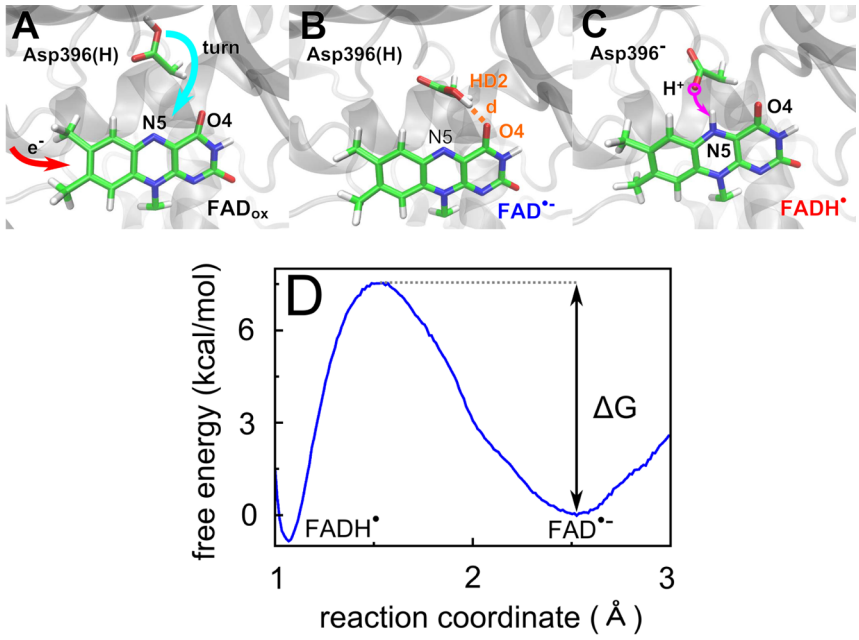

Figure 7. Protonation of flavin by D396. Shown is the spontaneous rotation of the COOH group of D396(H) toward flavin subsequent to the radical pair formation which ultimately leads to flavin protonation. Relative orientations of D396 and flavin obtained through MD simulation of (A) the resting state of cryptochrome and (B) cryptochrome in the radical pair state [$FAD^{\bullet-}$+$W400(H)^{\bullet+}$]. A hydrogen bond (orange) is formed between $D396^{HD2}$ and $flavin^{O4}$. Protonated flavin (C) is obtained from a QM/MM umbrella sampling calculation, which yields the energy profile (D) for flavin N5 protonation. The distance between the hydrogen of the COOH group and the flavin N5 atom was considered as the reaction coordinate.

electronic coupling renders the electron transfer from W_C to $W_B(H)^{\bullet+}$ almost impossible and provides a structural mechanism for the stabilization of RP-B against the solvent driving force. Note that electron back transfer $W_B(H)^{\bullet+} \rightarrow W_A$ is still possible but expected to be slow, due to the energetically more favorable stabilization of RP-B compared to RP-A, see Figure 4.

No additional mechanism for the stabilization of RP-A and RP-C has been observed for *A. thal.* cryptochrome. In a previous study on *E. coli* photolyase, a similar structural stabilization mechanism was discovered for RP-C.[61] Several nanoseconds after the RP-C was formed, a spontaneous increase of the distance and decrease of the electronic coupling between W_B and $W_C(H)^{\bullet+}$ was observed, essentially blocking the possibility of the $W_C(H)^{\bullet+} \rightarrow W_B$ electron back transfer.

Protonation of Flavin via D396. Triggered by the electron transfer event, a proton transfer from D396 to FAD was reported for *A. thal.* cryptochrome[33,36,83] which can further stabilize the ionic radical pair $FAD^{\bullet-}$+$W(H)^{\bullet+}$. Most recently, Müller and co-workers found that the rate of flavin protonation can be modulated by ATP binding and pH.[84,85] In the case of low pH and ATP absence they observed some ultrafast protonation of flavin, although the probability for millisecond flavin protonation was still found to be higher. A QM analysis of the active site[56] had also suggested flavin protonation to happen ultrafast and, therefore, to outrun the second electron transfer step along the tryptophan triad, potentially. Similarly to the description of the electron transfer process, however, a completed inclusion of the protein environment and solvent is necessary in order to obtain a balanced description of the proton transfer energetics and to unambigously determine whether the electron transfer along the tryptophan triad exceeds flavin protonation. Here, we use QM/MM umbrella sampling simulations including the complete protein and solvent environment in order to calculate the activation energy for protonation of flavin.

Recently,[56] it was shown that D396(H) is involved in a structural transformation once the flavin gains a negative charge and W_A becomes positively charged, and this might catalyze the protonation of flavin N5 via D396(H). In order to study the structural rearrangement subsequent to the formation of the primary radical pair [$FAD^{\bullet-}$+$W400(H)^{\bullet+}$], we conducted 14 classical MD simulations starting from different structures taken from the simulation of the cryptochrome resting state. The upper panel of Figure 7 shows that after the formation of the radical pair, the COOH group of the D396(H) residue turns spontaneously toward the flavin, and the COOH group approaches the N5 and O4 atoms of the flavin group, see Figure 7B. Then, a hydrogen bond of a 1.8 Å length is formed between the O4 atom of the flavin and the COOH group of D396.

The free energy profile for the protonation reaction of the flavin by D396 was obtained from a QM/MM umbrella sampling simulation where the hydrogen of the COOH group of D396 was pulled toward the N5 of the flavin group. The distance between the hydrogen of D396 and N5 atom of the flavin group was considered as the reaction coordinate and was sampled from 2.6 Å down to 0.9 Å to describe the proton transfer process completely. The WHAM calculation yielded a PMF with a minimum for the D396 hydrogen bonded to the flavin O4 and another minimum, which was 1.5 kcal/mol deeper, located at the protonated flavin state. The free energy barrier for the proton transfer amounted to 7.5 kcal/mol, see Figure 7D.

In the framework of the transition state theory,[86] the rate for the proton transfer can be estimated as

DOI: 10.1021/ja510550g
J. Am. Chem. Soc. 2015, 137, 1147–1156

$$k = \frac{k_B T}{h}(1 - e^{-h\nu/k_B T})e^{-\Delta G/k_B T} \quad (6)$$

where T denotes the temperature, ΔG is the free energy barrier, ν is the attempt frequency by which the transition state occurs, k_B is the Boltzmann constant and h is Planck's constant. The attempt frequency can be estimated as

$$\nu = \frac{1}{2\pi}\sqrt{\frac{k_{H-N}}{m_H}} \quad (7)$$

where $k_{H-N} \simeq 537$ ((kcal)/(mol Å^2)) is the H−N bond force constant (the characteristic value of the force constant in the CHARMM force field[73,74]), and m_H is the mass of the hydrogen atom. With eq 7 one thus obtains $\nu = 7.5 \times 10^{13}$ s^{-1}. Together with the free energy barrier of $\Delta G = 7.5$ kcal/mol, see Figure 7D, this leads to a rate constant of $k = 2.2 \times 10^7$ s^{-1}, which is equivalent to a time constant of 45 ns. This time constant can be understood as an estimate for the time it takes for the flavin to become protonated on average. In contrast, the electron transfer through the triad was found to proceed with a rate of about 2×10^{11} s^{-1} (a time constant of about 50 ps), as demonstrated above.

This analysis reveals that the proton transfer in *A. thal.* cryptochrome is expected to happen at least 4 orders of magnitude slower than the electron transfer. In a previous study,[56] the protonation time was estimated to be about 1 ns, which is faster than the present estimate, but still significantly slower than the electron transfer discussed above. Femtosecond spectroscopy experiments observed the proton transfer to the flavin with a time constant of about 1.7 μs[36] and the electron transfer along the tryptophan triad to be completed within 100 ps.[42] While our theoretical investigation yields electron transfer rates in an excellent agreement with the experiment, the findings for the proton transfer rate should be considered qualitative. It should also be noted that the rate of flavin protonation apparently depends on various external factors, such as pH and presence of charged cofactors around cryptochrome active site.[84,85] Note that the flavin protonation for the RP-A state was studied here in order to investigate if it could outrun the $W_B \rightarrow W_A(H)^{\bullet+}$ electron transfer process. However, since the electron transfer occurs significantly faster than the flavin protonation, the RP-C state will be formed, which would change the flavin protonation barrier. The barrier for flavin protonation in the RP-C state will likely be somewhat higher than in the case of the RP-A state, as it will be dominated by the pulling force from the negative flavin radical only, while in the case of the RP-A state the positively charged $W_A(H)^{\bullet+}$ radical additionally accelerates the flavin protonation process. The performed analysis proves clearly that the electron and proton transfer processes in plant cryptochrome are separated in time by several orders of magnitude. The protein environment imposes an activation barrier on flavin protonation ensuring the formation of the much more persistent radical pair $FAD^{\bullet-} + W_C(H)^{\bullet+}$, which is well separated in space, before the flavin protonation could occur.

CONCLUSION AND DISCUSSION

Cryptochrome is thought to host, upon light absorption, a radical pair that allows the protein to sense very weak magnetic fields, endowing migratory birds with a magnetic compass sense. The radical pair is formed in cryptochrome through a series of electron transfer reactions involving three tryptophan residues which are conserved throughout the cryptochrome/photolyase family. These radicals were shown to be likely sensitive to a weak magnetic field.[35] Here, we reveal the molecular driving force that ensures fast electron transfer along the tryptophan triad and guarantees the formation of a persistent radical pair suitable for magnetoreception.

Direct electron transfer simulations, which include the complete protein and solvent environments, show that two sequential electron transfers $W_B \rightarrow W_A^{\bullet+}$ and $W_C \rightarrow W_B^{\bullet+}$ lead to the stabilization of the radical pair RP-C or RP-B within 150 ps. The computed electron transfer rates are in excellent agreement with the experimental kinetics obtained from femtosecond spectroscopy[42] and provide an in-depth understanding of the photoactivation mechanism of plant cryptochrome. Analysis of the relative energies of the radical pair states RP-A, RP-B and RP-C reveals that the driving force results solely from differential solvation effects, i.e., from the fact that W_C is much more solvent exposed than W_A: the polarization of the solvent induces stabilization of RP-C by 0.8 eV with respect to RP-A. It is this strong exothermicity that renders the electron transfer to be very fast, stabilizes the radical pair and slows down electron back transfer reactions along the tryptophan triad.

A solvent-driven electron transfer along the tryptophan triad, inducing the stabilization of RP-C, was also found earlier in *E. coli* photolyase.[61,62] Given the fact that the tryptophan triad is conserved throughout the cryptochrome/photolyase family, our findings suggest that the solvent driving force is a general principle governing the fast electron transfer process of the photoactivation reaction in members of the cryptochrome/photolyase family. It represents the main feature that allows the formation of a radical pair, comprising all the essential prerequisites (fast formation, well separated in space, stabilized to prevent back transfer) for the potential sensitivity to weak magnetic fields.

Furthermore, the present study establishes a functional role of solvent for biological reactions. For both *A. thal.* cryptochrome and *E. coli* photolyase we have found an additional structural "locking" mechanism which enforces the electron reaction to be one-way, in addition to the stabilization already provided by the strong exothermicity of the reaction itself. This mechanism provides additional stabilization of RP-C on the nanosecond time scale in *E. coli* photolyase, while it allows stabilization of RP-B in *A. thal.* cryptochrome, each time allowing to fine-tune the radical pair stabilization specific to the function of the individual protein.

No doubt that the proposed magnetoreceptive function of cryptochrome[11,18,35] is an intriguing property of the protein, as it attracts the attention of an increasing number of researchers. It has been suggested[35] that an applied magnetic field influences the radical pair recombination reaction, which in turn competes with the tryptophan radical deprotonation reaction, see Figure 2. Interestingly, the magnetic field effect in *A. thal.* cryptochrome was observed to be about three times higher compared to *E. coli* photolyase.[35] The present investigation provides a qualitative answer to this observation.

The "locking" mechanism in *E. coli* photolyase leads to an additional, nanosecond stabilization of the RP-C state which does not permit the electron back transfer easily, thereby rendering the influence of an applied magnetic field on the probability of radical pair recombination less important, as the radical pair recombination is significantly decreased. In contrast, the "locking" mechanism in *A. thal.* cryptochrome helps to

DOI: 10.1021/ja510550g
J. Am. Chem. Soc. 2015, 137, 1147−1156

stabilize RP-B, but it does not prevent the recombination of RP-C specifically. Thus, since radical pair recombination is possible in *A. thal.* cryptochrome, the magnetic field could induce an increased recombination of the radical pair, resulting in a higher sensitivity of *A. thal.* cryptochrome compared to *E. coli* photolyase. This is in accord with the data of Maeda et al.[35] who estimated the rate constant for radical pair recombination to be $4.9 \times 10^5\ s^{-1}$ for *A. thal.* cryptochrome and $1.2 \times 10^5\ s^{-1}$ for *E. coli* photolyase. One might also speculate that the "locking" mechanism in *A. thal.* cryptochrome is tailor-made to allow stabilization of RP-B without additionally preventing radical pair recombination. This potentially permits a comparably high sensitivity of *A. thal.* cryptochrome to weak magnetic fields.

The present investigation completes the description of the photoactivation process along the tryptophan triad of plant cryptochrome. It provides the essential proof that a fast radical pair separation in cryptochrome to a functionally critical distance is possible, such that the protein potentially could function as an efficient sensor of weak magnetic fields. This peculiar functionality was postulated numerous times in earlier studies,[55,56] but the present investigation is the first to carry out a systematic and complete proof that a well-separated radical pair in cryptochrome exists. It is also worth mentioning that alternative, tyrosine-based, radical pairs in cryptochtome might exist.[87] Biskup et al. found a secondary electron transfer pathway along tyrosine resdiues in an amphibian cryptochrome that may provide an alternative photoactivation mechanism independent of the tryptophan triad and could explain why interrupting the conserved tryptophan triad does not necessarily alter photoreactions of cryptochromes in vivo. Further computational and experimental studies that investigate alternative radical pairs in mutants and their sensitivity to weak magnetic fields are called for to complete the understanding of radical pair formation in cryptochrome. Finally, the results of the present investigation permit to challenge the ultimate grand question related to cryptochrome signaling: How much does the weak magnetic field change its biological function? We are certain that by combining experimental efforts and modern computational techniques, this question will be unraveled in the nearest future.

■ ASSOCIATED CONTENT

Supporting Information

We present details of theoretical methods used for the calculations. Additionally, Supplementary Table S1, Supplementary Figures S1 and S2, Supplementary Files, and Supplementary Movies are also available. This material is available free of charge via the Internet at http://pubs.acs.org.

■ AUTHOR INFORMATION

Corresponding Authors

ilia@sdu.dk

marcus.elstner@kit.edu

Notes

The authors declare no competing financial interest.

■ ACKNOWLEDGMENTS

The authors acknowledge supercomputer time on Stampede provided by the Texas Advanced Computing Center (TACC) at the University of Texas at Austin through Extreme Science and Engineering Discovery Environment (XSEDE) Grant XSEDE MCB-120160. IAS is grateful for the financial support from the Lundbeck Foundation, and the Russian Scientific Foundation (Grant No. 14-12-00342).

■ REFERENCES

(1) Guerra, P.; Gegear, R.; Reppert, S. *Nat. Commun.* **2014**, *5*, 4164.
(2) Phillips, J. B.; Jorge, P. E.; Muheim, R. *J. R. Soc., Interface* **2010**, *7*, 241−256.
(3) Lohmann, K.; Lohmann, C.; Erhart, L.; Bagley, D.; Swing, T. *Nature* **2004**, *428*, 909−910.
(4) Lohmann, K. J.; Putmann, N. F.; Lohmann, C. M. F. *Proc. Natl. Acad. Sci. U. S. A.* **2008**, *105*, 19096−19101.
(5) Wiltschko, W.; Wiltschko, R. *Science* **1972**, *176*, 62−64.
(6) Mouritsen, H.; Janssen-Bienhold, U.; Liedvogel, M.; Feenders, G.; Stalleicken, J.; Dirks, P.; Weiler, R. *Proc. Natl. Acad. Sci. U. S. A.* **2004**, *101*, 14294−14299.
(7) Johnsen, S.; Lohmann, K. J. *Phys. Today* **2008**, *61*, 29−35.
(8) Ball, P. *Nature* **2011**, *474*, 272−274.
(9) Brautigam, C. A.; Smith, B. S.; Ma, Z.; Palnitkar, M.; Tomchick, D. R.; Machius, M.; Deisenhofer, J. *Proc. Natl. Acad. Sci. U. S. A.* **2004**, *101*, 12142−12147.
(10) Solov'yov, I. A.; Hore, P. J.; Ritz, T.; Schulten, K. In *Quantum Effects in Biology*; Mohseni, M., Omar, Y., Engel, G., Plenio, M. B., Eds.; Cambridge University Press: Cambridge, 2014; Chapter A Chemical Compass for Bird Navigation, pp 218−236.
(11) Ritz, T.; Adem, S.; Schulten, K. *Biophys. J.* **2000**, *78*, 707−718.
(12) Rodgers, C.; Hore, P. J. *Proc. Natl. Acad. Sci. U. S. A.* **2009**, *106*, 353−360.
(13) Solov'yov, I. A.; Mouritsen, H.; Schulten, K. *Biophys. J.* **2010**, *99*, 40−49.
(14) Solov'yov, I. A.; Schulten, K.; Greiner, W. *Phys. J.* **2010**, *5*, 23−28.
(15) Solov'yov, I. A.; Schulten, K. *Biophys. J.* **2009**, *96*, 4804−4813.
(16) Liedvogel, M.; Mouritsen, H. *J. R. Soc., Interface* **2010**, *7*, S147−S162.
(17) Solov'yov, I. A.; Chandler, D. E.; Schulten, K. *Biophys. J.* **2007**, *92*, 2711−2726.
(18) Lee, A. A.; Lau, J. C.; Hogben, H. J.; Biskup, T.; Kattnig, D. R.; Hore, P. J. *J. R. Soc., Interface* **2014**, *11*, 20131063.
(19) Nießner, C.; Denzau, S.; Gross, J. C.; Peichl, L.; Bischof, H.-J.; Fleissner, G.; Wiltschko, W.; Wiltschko, R. *PLoS One* **2011**, *6*, e20091.
(20) Ahmad, M.; Cashmore, A. R. *Plant Mol. Biol.* **1996**, *30*, 851−861.
(21) Sancar, A.; Lindsey-Boltz, L.; Kang, T.; Reardon, J.; Lee, J.; Ozturk, N. *FEBS Lett.* **2010**, *584*, 2618−2625.
(22) Dodson, C. A.; Hore, P.; Wallace, M. I. *Trends Biochem. Sci.* **2013**, *38*, 435−446.
(23) Cashmore, A. R.; Jarillo, J. A.; Wu, Y.-J.; Liu, D. *Science* **1999**, *284*, 760−765.
(24) Partch, C. L.; Sancar, A. *Methods Enzymol.* **2005**, *393*, 726−745.
(25) Yoshii, T.; Ahmad, M.; Helfrich-Foerster, C. *PLoS Biol.* **2009**, *7*, 813−819.
(26) Chaves, I.; Pokorny, R.; Byrdin, M.; Hoang, N.; Ritz, T.; Brettel, K.; Essen, L.-O.; van der Horst, G. T.; Batschauer, A.; Ahmad, M. *Annu. Rev. Plant Biol.* **2011**, *62*, 335−364.
(27) Ahmad, M.; Galland, P.; Ritz, T.; Wiltschko, R.; Wiltschko, W. *Planta* **2007**, *225*, 615−624.
(28) Zantke, J.; Ishikawa-Fujiwara, T.; Arboleda, E.; Lohs, C.; Schipany, K.; Hallay, N.; Straw, A.; Todo, T.; Tessmar-Raible, K. *Cell Rep.* **2013**, *5*, 99−113.
(29) Levy, O.; Appelbaum, L.; Leggat, W.; Gothlif, Y.; Hayward, D. C.; Miller, D. J.; Hoegh-Guldberg, O. *Science* **2007**, *318*, 467−470.
(30) Fukushiro, M.; Takeuchi, T.; Takeuchi, Y.; Hur, S.-P.; Sugama, N.; Takemura, A.; Kubo, Y.; Okano, K.; Okano, T. *PLoS One* **2011**, *6*, e28643.
(31) Giovani, B.; Byrdin, M.; Ahmad, M.; Brettel, K. *Nat. Struct. Biol.* **2003**, *10*, 489−490.

DOI: 10.1021/ja510550g
J. Am. Chem. Soc. 2015, 137, 1147−1156

(32) Zeugner, A.; Byrdin, M.; Bouly, J.-P.; Bakrim, N.; Giovani, B.; Brettel, K.; Ahmad, M. *J. Biol. Chem.* **2005**, *280*, 19437−19440.
(33) Kottke, T.; Batschauer, A.; Ahmad, M.; Heberle, J. *Biochemistry* **2006**, *45*, 2472−2479.
(34) Biskup, T.; Schleicher, E.; Okafuji, A.; Link, G.; Hitomi, K.; Getzoff, E. D.; Weber, S. *Angew. Chem., Int. Ed. Engl.* **2009**, *48*, 404−407.
(35) Maeda, K.; Robinson, A. J.; Henbest, K. B.; Hogben, H. J.; Biskup, T.; Ahmad, M.; Schleicher, E.; Weber, S.; Timmel, C. R.; Hore, P. J. *Proc. Natl. Acad. Sci. U. S. A.* **2012**, *109*, 4774−4779.
(36) Langenbacher, T.; Immeln, D.; Dick, B.; Kottke, T. *J. Am. Chem. Soc.* **2009**, *131*, 14274−14280.
(37) Zoltowski, B.; Vaidya, A.; Top, D.; Widom, J.; Young, M.; Crane, B. *Nature* **2011**, *480*, 396−399.
(38) Zoltowski, B.; Vaidya, A.; Top, D.; Widom, J.; Young, M.; Crane, B. *Nature* **2013**, *496*, 252.
(39) Czarna, A.; Berndt, A.; Singh, H. R.; Grudziecki, A.; Ladurner, A. G.; Timinszky, G.; Kramer, A.; Wolf, E. *Cell* **2013**, *153*, 1394−1405.
(40) Shirdel, J.; Zirak, P.; Penzkofer, A.; Breitkreuz, H.; Wolf, E. *Chem. Phys.* **2008**, *352*, 35−47.
(41) Liedvogel, M.; Maeda, K.; Henbest, K.; Schleicher, E.; Simon, T.; Timmel, C. R.; Hore, P.; Mouritsen, H. *PLoS One* **2007**, *2*, e1106.
(42) Immeln, D.; Weigel, A.; Kottke, T.; Lustres, J. L. P. *J. Am. Chem. Soc.* **2012**, *134*, 12536−12546.
(43) Hein, C. M.; Engels, S.; Kishkinev, D.; Mouritsen, H. *Nature* **2011**, *471*, E11−E12.
(44) Gegear, R. J.; Casselman, A.; Waddell, S.; Reppert, S. M. *Nature* **2008**, *454*, 1014−1018.
(45) Gegear, R. J.; Foley, L. E.; Casselman, A.; Reppert, S. M. *Nature* **2010**, *463*, 804−807.
(46) Foley, L. E.; Gegear, R. J.; Reppert, S. M. *Nat. Commun.* **2011**, *2*, 356.
(47) Lauwers, M.; Pichler, P.; Edelman, N.; Resch, G.; Ushakova, L.; Salzer, M.; Heyers, D.; Saunders, M.; Shaw, J.; Keays, D. *Curr. Biol.* **2013**, *23*, 924−929.
(48) Treiber, C.; Salzer, M.; Breuss, M.; Ushakova, L.; Lauwers, M.; Edelman, N.; Keays, D. *Commun. Integr. Biol.* **2013**, *6*, e24859.
(49) Treiber, C.; Salzer, M.; Riegler, J.; Edelman, N.; Sugar, C.; Breuss, M.; Pichler, P.; Cadiou, H.; Saunders, M.; Lythgoe, M.; Shaw, J.; Keays, D. *Nature* **2012**, *484*, 367−370.
(50) Fleissner, G.; Stahl, B.; Thalau, P.; Falkenberg, G.; Fleissner, G. *Naturwissenschaften* **2007**, *94*, 631−642.
(51) Solov'yov, I. A.; Greiner, W. *Phys. Rev. E: Stat., Nonlinear, Soft Matter Phys.* **2009**, *80*, 041919.
(52) Solov'yov, I. A.; Greiner, W. *Eur. Phys. J. D* **2009**, *51*, 161−172.
(53) Solov'yov, I. A.; Greiner, W. *Biophys. J.* **2007**, *93*, 1493−1509.
(54) Falkenberg, G.; Fleissner, G.; Schuchardt, K.; Kuehbacher, M.; Thalau, P.; Mouritsen, H.; Heyers, D.; Wellenreuther, G.; Fleissner, G. *PLoS One* **2010**, *5*, e9231.
(55) Solov'yov, I. A.; Domratcheva, T.; Schulten, K. *Sci. Rep.* **2014**, *4*, 3845.
(56) Solov'yov, I. A.; Domratcheva, T.; Moughal Shahi, A. R.; Schulten, K. *J. Am. Chem. Soc.* **2012**, *134*, 18046−18052.
(57) Solov'yov, I. A.; Schulten, K. *J. Phys. Chem. B* **2012**, *116*, 1089−1099.
(58) Kubař, T.; Elstner, M. *J. Phys. Chem. B* **2010**, *114*, 11221−11240.
(59) Kubař, T.; Elstner, M. *Phys. Chem. Chem. Phys.* **2013**, *15*, 5794−5813.
(60) Kubař, T.; Elstner, M. *J. R. Soc., Interface* **2013**, *10*, 20130415.
(61) Woiczikowski, P. B.; Steinbrecher, T.; Kubař, T.; Elstner, M. *J. Phys. Chem. B* **2011**, *115*, 9846−9863.
(62) Lüdemann, G.; Woiczikowski, P. B.; Kubař, T.; Elstner, M.; Steinbrecher, T. B. *J. Phys. Chem. B* **2013**, *117*, 10769−10778.
(63) Hess, B.; Kutzner, C.; van der Spoel, D.; Lindahl, E. *J. Chem. Theory Comput.* **2008**, *4*, 435−447.
(64) Wang, J.; Wolf, R. M.; Caldwell, J. W.; Kollman, P. A.; Case, D. A. *J. Comput. Chem.* **2004**, *25*, 1157−1174.
(65) Hornak, V.; Abel, R.; Okur, A.; Strockbine, B.; Roitberg, A.; Simmerling, C. *Proteins: Struct., Funct., Genet.* **2006**, *65*, 712−725.
(66) Gaus, M.; Cui, Q.; Elstner, M. *J. Chem. Theory Comput.* **2011**, *7*, 931−948.
(67) Humphrey, W.; Dalke, A.; Schulten, K. *J. Mol. Graphics* **1996**, *14*, 33−38.
(68) Meagher, K. L.; Redman, L. T.; Carlson, H. A. *J. Comput. Chem.* **2003**, *24*, 1016−1025.
(69) Bayly, C. I.; Cieplak, P.; Cornell, W. D.; Kollman, P. A. *J. Phys. Chem.* **1993**, *97*, 10269−10280.
(70) Song, Y.; Mao, J.; Gunner, M. R. *J. Comput. Chem.* **2009**, *30*, 2231−2247.
(71) Jorgensen, W. L.; Chandrasekhar, J.; Madura, J. D.; Impey, R. W.; Klein, M. L. *J. Chem. Phys.* **1983**, *79*, 926−935.
(72) Phillips, J. C.; Braun, R.; Wang, W.; Gumbart, J.; Tajkhorshid, E.; Villa, E.; Chipot, C.; Skeel, R. D.; Kale, L.; Schulten, K. *J. Comput. Chem.* **2005**, *26*, 1781−1802.
(73) MacKerell, A. D., Jr.; Bashford, D.; Bellott, M.; Dunbrack, R. L., Jr.; Evanseck, J. D.; Field, M. J.; Fischer, S.; Gao, J.; Guo, H.; Ha, S.; Joseph, D.; Kuchnir, L.; Kuczera, K.; Lau, F. T. K.; Mattos, C.; Michnick, S.; Ngo, T.; Nguyen, D. T.; Prodhom, B.; Reiher, I. W. E.; Roux, B.; Schlenkrich, M.; Smith, J.; Stote, R.; Straub, J.; Watanabe, M.; Wiorkiewicz-Kuczera, J.; Yin, D.; Karplus, M. *J. Phys. Chem. B* **1998**, *102*, 3586−3616.
(74) MacKerell, A. D., Jr.; Feig, M.; Brooks, C. L., III *J. Comput. Chem.* **2004**, *25*, 1400−1415.
(75) Evans, D. J.; Holian, B. L. *J. Chem. Phys.* **1985**, *83*, 4069−4074.
(76) Parinello, M.; Rahman, A. *J. Appl. Phys.* **1981**, *52*, 7182−7190.
(77) Hess, B.; Bekker, H.; Berendsen, H. J. C.; Fraaije, J. G. E. M. *J. Comput. Chem.* **1997**, *18*, 1463−1472.
(78) Kitaura, K.; Ikeo, E.; Asada, T.; Nakano, T.; Uebayasi, M. *Chem. Phys. Lett.* **1999**, *313*, 701−706.
(79) Elstner, M.; Porezag, D.; Jungnickel, G.; Elsner, J.; Haugk, M.; Frauenheim, T.; Suhai, S.; Seifert, G. *Phys. Rev. B: Condens. Matter Mater. Phys.* **1998**, *58*, 7260−7268.
(80) Gaus, M. *J. Chem. Theory Comput.* **2013**, *9*, 931−948.
(81) Hub, J. S.; de Groot, B. L.; van der Spoel, D. *J. Chem. Theory Comput.* **2010**, *6*, 3713−3720.
(82) Sancar, A. *Chem. Rev.* **2003**, *103*, 2203−2237.
(83) Brettel, K.; Byrdin, M. *Curr. Opin. Struct. Biol.* **2010**, *20*, 693−701.
(84) Müller, P.; Bouly, J. P.; Hitomi, K.; Balland, E. D.; Getzoff, V.; Ritz, T.; Brettel, K. *Sci. Rep.* **2014**, *4*, 5175.
(85) Caillez, F.; Müller, P.; Gallois, M.; de la Lande, A. *J. Am. Chem. Soc.* **2014**, *136*, 12974−12986.
(86) Herzfeld, K. F. *Ann. Phys.* **1919**, *59*, 635−667.
(87) Biskup, T.; Paulus, B.; Okafuji, A.; Hitomi, K.; Getzoff, E. D.; Weber, S.; Schleicher, E. *J. Biol. Chem.* **2013**, *288*, 9249−9260.

DOI: 10.1021/ja510550g
J. Am. Chem. Soc. 2015, 137, 1147−1156